J Nanostruct 10(2): 239-257, Spring 2020

RESEARCH PAPER

Enhanced Catalytic Activity of Pt-$NdFeO_3$ Nanoparticles Supported on Polyaniline-Chitosan Composite Towards Methanol Electro-Oxidation Reaction

Somaye Khammarnia [1], Alireza Akbari [1], Mehri-Saddat Ekrami-Kakhki [2] and Jilla Saffari [3]*

[1] *Chemistry Department, Payame Noor University, Tehran, Iran*

[2] *Central Research Laboratory, Esfarayen University of Technology, Esfarayen, North Khorasan, Iran*

[3] *Department of Chemistry, Zahedan Branch, Islamic Azad University, Zahedan, Iran*

ARTICLE INFO

Article History:
Received 03 December 2019
Accepted 22 February 2020
Published 01 April 2020

Keywords:
Chitosan
Methanol Electro-oxidation
$NdFeO_3$
Polyaniline

ABSTRACT

In this work, $NdFeO_3$ nanoparticles were synthesized through a simple co-precipitation method. The formation of $NdFeO_3$ particles was verified by X-ray powder diffraction, infrared spectroscopy, vibrating sample magnetometer, and transmission electron microscopy analysis. Polyaniline and chitosan were employed as proper support for production of metal nanoparticles. Novel Pt-NFO/PA-CH nanocomposite was fabricated by immobilization of Pt nanoparticles on the PA-CH support in the presence of $NdFeO_3$ nanoparticles. The prepared nanocomposite was characterized by transmission electron microscopy and X-ray powder diffraction analysis. The catalytic performance of the Pt-NFO/PA-CH nanocomposite was evaluated for electro-oxidation of methanol through CO stripping voltammetry, cyclic voltammetry, chronoamperometry, and electrochemical impedance spectroscopy. Durability of the Pt-NFO/PA-CH catalyst was investigated and the effects of several factors such as temperature, scan rate, and methanol concentration were studied for methanol oxidation. Enhanced catalytic performance of Pt-NFO/PA-CH nanocatalyst compared to Pt/PA-CH catalyst recommends its application for methanol electro-oxidation in direct methanol fuel cells.

How to cite this article
Khammarnia S, Akbari A, Ekrami-Kakhki M, Saffari J. Enhanced Catalytic Activity of Pt-$NdFeO_3$ Nanoparticles Supported on Polyaniline-Chitosan Composite Towards Methanol Electro-Oxidation Reaction. J Nanostruct, 2020; 10(2):239-257. DOI: 10.22052/JNS.2020.02.005

INTRODUCTION

Today, the use of fossil fuels has been limited due to the pollution of their combustion and the limited sources. To meet the energy demands of the world, scientists are looking for the new alternative energy sources. Recently, direct methanol fuel cells (DMFCs) have been considered as new, renewable and clean energy sources due to their simplicity, high efficiency, simply fuel storage, low pollution, and high energy densities [1-4]. DMFCs are new generation of the fuel cells which operate on the basis of direct oxidation of methanol as fuel [5, 6]. Methanol has several advantages as a liquid fuel such as easy availability, simple storage, handling and transportation, and high energy density. Among noble metals, platinum has greater catalytic activity for methanol oxidation reaction (MOR) [7, 8] but its high price and easily poisoning with carbon monoxide (CO) as byproduct of MOR constrain its widespread utilization [9]. CO intermediates can strongly be adsorbed at the Pt nanoparticles' surface and poison it for electro-oxidation of methanol [10, 11].

To develop new anode catalysts with excellent activity for MOR in DMFCs, to reduce the amount

* *Corresponding Author Email: ekrami@esfarayen.ac.ir*

of Pt loading and to reduce its poisoning effect, structure of support material and also composition of Pt-based catalysts are very important [12-17]. Extensive researches have been done in developing the promising catalysts for DMFCs through alloying Pt with other metals and modifying the electronic structure of Pt catalysts [18-26]. In DMFCs, Pt-based catalysts have lower cost, improved antipoisoning effect, and enhanced catalytic activity towards electro-oxidation of methanol compared with pure Pt catalyst [27-29]. For example different metal oxides such as, Ce, Pr, Nd and Sm oxides incorporated on mesoporous carbon have been utilized to enhance the performance of Pt nanoparticles for MOR [30]. Amin used Pt-CuO/C catalyst for MOR [31]. Rare earth oxides have been used to modify Pt/C electrocatalysts for MOR [32], and Pt-Fe nanoparticles supported on reduced graphene oxides have been used for methanol electro-oxidation [33]. $NdFeO_3$ catalysts have been used for various chemical reactions. For example, $PrFeO_3$ and $NdFeO_3$ thick films have been synthesized and used for CO_2 sensing [34]. Palladium doped $NdFeO_3$ catalysts have been used for their acetone-sensing properties [35]. Pt nanoparticles doped on $NdFeO_3$ and carbon nanotubes have been utilized for polymeric fuel cells [36]. The performance of Palladium nanoparticles accompanied by $NdFeO_3$ perovskite has been investigated for direct methanol alkaline fuel cells [37].

A simple and effective method to enhance the performance of Pt catalysts is dispersing Pt nanoparticles on a conductive material as support. Several kinds of carbon support materials including graphene [38], carbon nanotubes [39], carbon vulcans [40], functionalized reduced graphene oxide [41], carbon blacks [42], carbon nanofibers [43], and conducting polymers [44-46] are common supports for metal nanoparticles in the fuel cell applications. Conducting polymers such as poly (o-toluidine) [47], polyaniline (PA) [48, 49], poly (o-methoxyaniline) [50], polypyrrole [51-53], and their derivatives are known as proper supporting materials for metal nanoparticles due to their high conductivity and large surface area. Polyaniline and its derivatives have attracted increasing attention as support for Pt nanoparticles due to their porous structure, large surface area, facil synthesis, and high chemical stability [54-56]. Chitosan (CH), a biopolymer produced by deacetylation of chitin, is used as support for metal nanoparticles in the fuel cells and shows strong affinity for transition metals [57].

Here, $NdFeO_3$ (NFO) nanoparticles were successfully synthesized and used accompanied by Pt nanoparticles to improve their catalytic activity for methanol electro-oxidation in acidic media. For the first time, Pt and NFO nanoparticles were dispersed on polyaniline and chitosan (PA-CH) support to prepare the novel Pt-NFO/PA-CH nanocatalyst in one step process. The catalytic performance of Pt-NFO/PA-CH nanocatalyst and also its CO-tolerance were studied for methanol electro-oxidation and compared with those of Pt/PA-CH. The effects of several experimental factors were investigated on the electrocatalytic performance of Pt-NFO/PA-CH for MOR. The durability of the prepared catalysts was also investigated for MOR. Pt-NFO/PA-CH nanocatalyst showed better poisoning resistance and considerably improved catalytic performance for MOR compared to Pt/PA-CH.

MATERIAL AND METHODS

$Fe(NO_3)_3.9H_2O$, $NdCl_3.6H_2O$, NaOH, and octanoic acid were prepared from Merck and used for synthesis of $NdFeO_3$ nanoparticles. Hexachloroplatinic acid and $NaBH_4$ (96%) were purchased from Merck and utilized to prepare Pt nanoparticles. H_2SO_4 (98% from Merck) was used as electrolyte. Polyaniline (PA) from Sigma-Aldrich and chitosan (CH) with medium molecular weight (Fluka) were utilized as support to prepare Pt-NFO/PA-CH nanocomposite. Acetic acid 1% (glacial, 100% Merck) solution was used for preparation of chitosan solution. Methanol (CH_3OH, 99.2%) was obtained from Merck and used for methanol oxidation (MO) investigation.

Preparation of NFO nanoparticles

To prepare NFO nanoparticles, 0.01 mole $NdCl_3.6H_2O$ and 0.01 mole $Fe(NO_3)_3.9H_2O$ were dissolved in 10 ml of deionized water. After the addition of 2 ml octanoic acid as surfactant, the solution was stirred vigorously while its pH was reached to 9 using NaOH 2 M. After complete precipitation, the obtained solution was irradiated with ultrasonic waves at 50°C for 60 min (250 W, 40 kHz). The resulting precipitate was centrifuged, washed, and dried at room temperature. The obtained powder was calcined at 600°C for 4 h. NFO nanoparticles were synthesized and characterized.

Synthesis of Pt-NFO/PA-CH nanocomposite

Pt-NFO/PA-CH nanocomposite was prepared through the following method: 1 mg PA was dispersed in the mixture of 17.5 ml deionized water and 2.5 ml chitosan and sonicated for 1 h. Then, 2 mg of the prepared NFO nanocatalysts was added to the above mixture and sonicated for 30 min to get the uniform dispersion of NFO nanoparticles. Afterwards, 25 µl H_2PtCl_6 was added to the solution and stirred magnetically for 1 h to obtain H_2PtCl_6 solution (0.00125 M). Then, 50 µl $NaBH_4$ (3M) was added rapidly. Having been stirred for 24 h, the black suspension was centrifuged and washed for several times. After drying at 60 ˚C for 12 h, Pt-NFO/PA-CH nanocomposite was obtained. Pt/PA-CH was prepared with the same procedure without using NFO nanoparticles.

Preparation of the electrodes

The modified working electrodes were prepared by mixing 2 mg of the corresponding catalyst powder in 1 ml chitosan solution. After sonication for 10 min, 5 µl of the suspension was transferred to the polished working electrode and dried at ambient temperature.

Characterization

An alternating gradient force magnetometer (AGFM) apparatus fabricated by Meghnatis Daghigh Kavir Co. (Iran) was used to investigate the room temperature magnetic property of the prepared NFO nanocatalyst, in an applied magnetic field sweeping between ± 10,000 Oe. The chemical components of the prepared catalysts were characterized by X-ray diffraction (XRD) using a Philips X-ray diffractometer with Ni-filtered CuK_α radiation. Fourier-transform infrared spectroscopy (FT-IR) spectra of NFO nanoparticles and octanoic acid were recorded on a Galaxy series FTIR5000 spectrophotometer. Transmission electron microscope (TEM) images taken with TEM (Zeiss - EM10C - 100 KV) were used to observe the morphology of catalysts. Ultrasonic irradiation of the samples was controlled by a multivalve ultrasonic generator (Band line MS 73), fitted out with a converter/transducer and titanium oscillator which operate at 20 kHz. The N2 adsorption/desorption isotherms were measured using a BET instrument (Belsorp mini II, BEL Japan Ins.) at the temperature of liquid nitrogen.

All electrochemical investigations were done using an Autolab potentiostat (PGSTAT 302N, Nova software, Metrohm, Netherlands). The modified glassy carbon (GC) electrodes with 2 mm diameter were utilized as working electrode. A saturated calomel electrode (SCE) and a platinum wire were respectively served as reference and counter electrodes. The inductively coupled plasma optical emission spectroscopy (ICP-OES) was employed to know the content of Pt nanoparticles on the surface of modified GC working electrodes.

RESULTS AND DISCUSSION

Catalyst characterization

The crystal structure of the synthesized catalysts was evaluated by XRD analysis (Fig. 1). XRD pattern of NFO shows the pure orthorhombic phase (a= 5.441, b=5.5730, c= 7.7) that is similar to the literature values (JCPDS No. 08-0168), with the main diffraction peak related to the (110) plane at d = 2.76 Å. Sharpening of the peaks is related to the high crystallinity of NFO catalyst. At Pt/PA-CH catalyst, the characteristics of PA peaks are similar to the XRD pattern of normal PA [58]. The diffraction peaks at 14.6˚, 27.96˚, and 31.68˚ are related to the (010), (111) and (022) planes of PA [59-62]. The diffraction peaks of Pt at 40.36˚, 45.36˚ and 67.36˚ are related to the (111), (200), and (220) planes of the cubic Pt, respectively [63]. Magnetic property of the prepared NFO was investigated by AGFM system at room temperature. The hysteresis loop of NFO nanocatalyst is illustrated in Fig. 1. Coercivity and saturation magnetization of NFO were about 100Oe and 1.24 emu g^{-1}, respectively. NFO nanoparticles show ferromagnetic behavior.

FTIR spectra of octanoic acid and the prepared NFO catalyst after calcination are shown in Fig. 2. For octanoic acid, the broad band at 2650-3450 cm^{-1} is related to the O-H stretching vibration of carboxylic acid. The peak at 1718 cm^{-1} is attributed to the carbonyl group. Two peaks at 1381 and 1461 cm^{-1} are related to the bending of CH_3 and CH_2 groups, respectively. The observed peak at 1220-1330 cm^{-1} is assigned to the stretching of C-O group and the absorption peak at 941 cm^{-1} is assigned to the out of plane bending of the O-H group [64]. In the FTIR spectrum of NFO nanocatalyst, there is a strong absorption band at nearly 789 cm^{-1} relating to the metal-O stretching vibration of NFO nanoparticles [65].

TEM analysis was used to know the particle size, and morphology of the catalysts. Fig. 2 represents TEM image of NFO nanocatalyst. As shown, NFO nanoparticles have spherical shape. TEM image

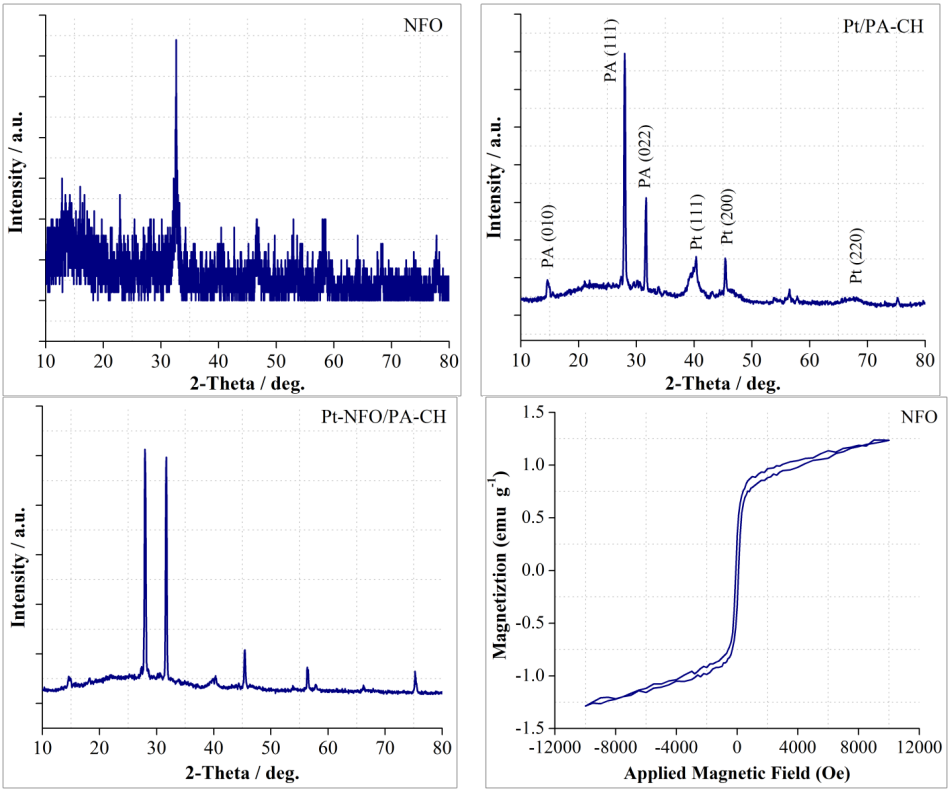

Fig. 1. XRD patterns of the prepared catalysts and room temperature hysteresis loop of NFO nanocatalyst.

of Pt/PA catalyst without chitosan is also shown in Fig. 2. The microstructure, distribution, and morphology of Pt and NFO nanoparticles on PA-CH support are shown by TEM images in Fig. 3. For Pt/PA-CH catalyst, it is observed that Pt nanoparticles with the mean particle size of 1.87 nm are dispersed uniformly on the matrix of PA-CH support and have low agglomeration. Comparing TEM images of Pt/PA (Fig. 2) and Pt/PA-CH (Fig. 3) demonstrates that in the absence of chitosan, more agglomeration would happen for Pt nanoparticles and the use of chitosan accompanied by PA lead to the better and more uniform distribution of Pt nanoparticles.

As shown for Pt-NFO/PA-CH catalyst in Fig. 3, Pt nanoparticles (mean particle size of 2.04 nm) are well dispersed on the matrix of PA-CH support and also around NFO nanoparticles (mean particle size of 19.92 nm) and have very low agglomeration. This uniform distribution of Pt nanoparticles is attributed to the use of polyaniline and chitosan as supporting materials. PA is a conducting polymer with NH functional groups in its structure. The presence of NH functional groups in PA and the amino groups in chitosan structure provides positive groups in acidic media. The electrostatic attraction between these positive functional groups and the negative charged $PtCl_6^{2-}$ (the precursor of Pt nanoparticles) causes the uniform dispersion of Pt particles. Furthermore, the use of CH as supporting material lead to the good adherence of the catalyst ink layer on the surface of GC electrode. The schematic illustration for preparing Pt-NFO/PA-CH nanocatalyst towards MOR is shown in Fig. 4.

The N2 adsorption/desorption isotherms were measured using a BET instrument (Belsorp mini II, BEL Japan Ins.) at the temperature of liquid nitrogen. The specific surface area was calculated by using the BET (Brunauer–Emmett–Teller) model [66] and the pore size distributions were determined by the BJH (Barrett–Joyner–Halenda) method [67].

The N_2 adsorption–desorption isotherm and pore size distribution of the $NdFeO_3$ nanoparticles was illustrated in Fig. 5. The BET surface area, total pore volume and pore diameter of NFO calculated from the desorption branch of the isotherm using the BJH method were 10.642 m^2g^{-1}, 0.0301 cm^3g^{-1}

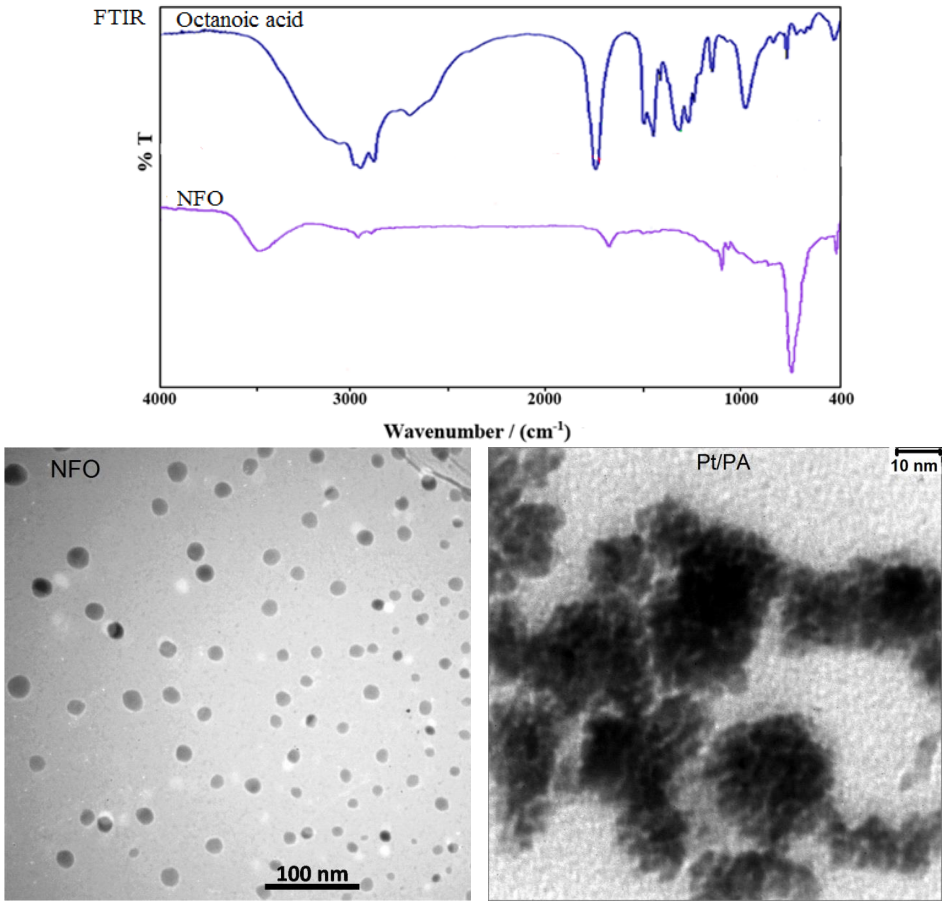

Fig. 2. FTIR spectra of octanoic acid and NFO nanocatalyst, TEM images of NFO nanoparticles and Pt/PA catalyst.

and 22.07 nm, respectively.

Electrocatalytic measurements

The electrochemical behavior of Pt/PA-CH and Pt-NFO/PA-CH nanocatalysts in a 0.5 M H_2SO_4 electrolyte was studied through cyclic voltammetry (CV) in the potential sweeps from -0.3 V to 1.2 V at 100 mV s^{-1} (Fig. 6A). The amount of platinum loading at the surface of GC electrode was 0.049 mg cm^{-2}. Both CV curves demonstrated hydrogen adsorption and hydrogen desorption peaks which can be served for calculation the electrochemically active surface area (EAS_H). The EAS_H value of each catalyst can be used to determine its electrocatalytic activity [68]. It is determined by calculating the charges of hydrogen adsorption and desorption peaks after excluding the effect of double-layer using the following equation [69]:

$$EAS_H = {}^{Q_H}/_{0.21 \times [Pt]} \quad (1)$$

0.21 mC cm^{-2} is the charge considered for oxidizing single layer of the adsorbed hydrogen on platinum [70], [Pt] is the amount of platinum loading on GC electrode and Q_H is the columbic charge for hydrogen adsorption/desorption on the Pt sites [70]. For Pt/PA-CH and Pt-NFO/PA-CH catalysts, Q_H was determined between -0.271 to 0.051 V vs. SCE. The EAS_H value of Pt-NFO/PA-CH catalyst (94.46 $m^2\ g^{-1}_{Pt}$) was more than Pt/PA-CH catalyst (75.83 $m^2\ g^{-1}_{Pt}$) demonstrating that Pt-NFO/PA-CH has higher electrocatalytic performance than Pt/PA-CH catalyst [71].

The CO poisoning resistance of Pt-NFO/PA-CH and Pt/PA-CH catalysts was determined by CO stripping voltammetry shown in Fig. 6B [72]. CO stripping experiment was performed by purging CO gas in H_2SO_4 0.5 M while the potential was held at 0.2 V for 20 min at 100 mV s^{-1}. Afterwards, N_2 gas was bubbled for 20 min to remove the non-adsorbed CO [73].

The CO oxidation peak of Pt-NFO/PA-CH

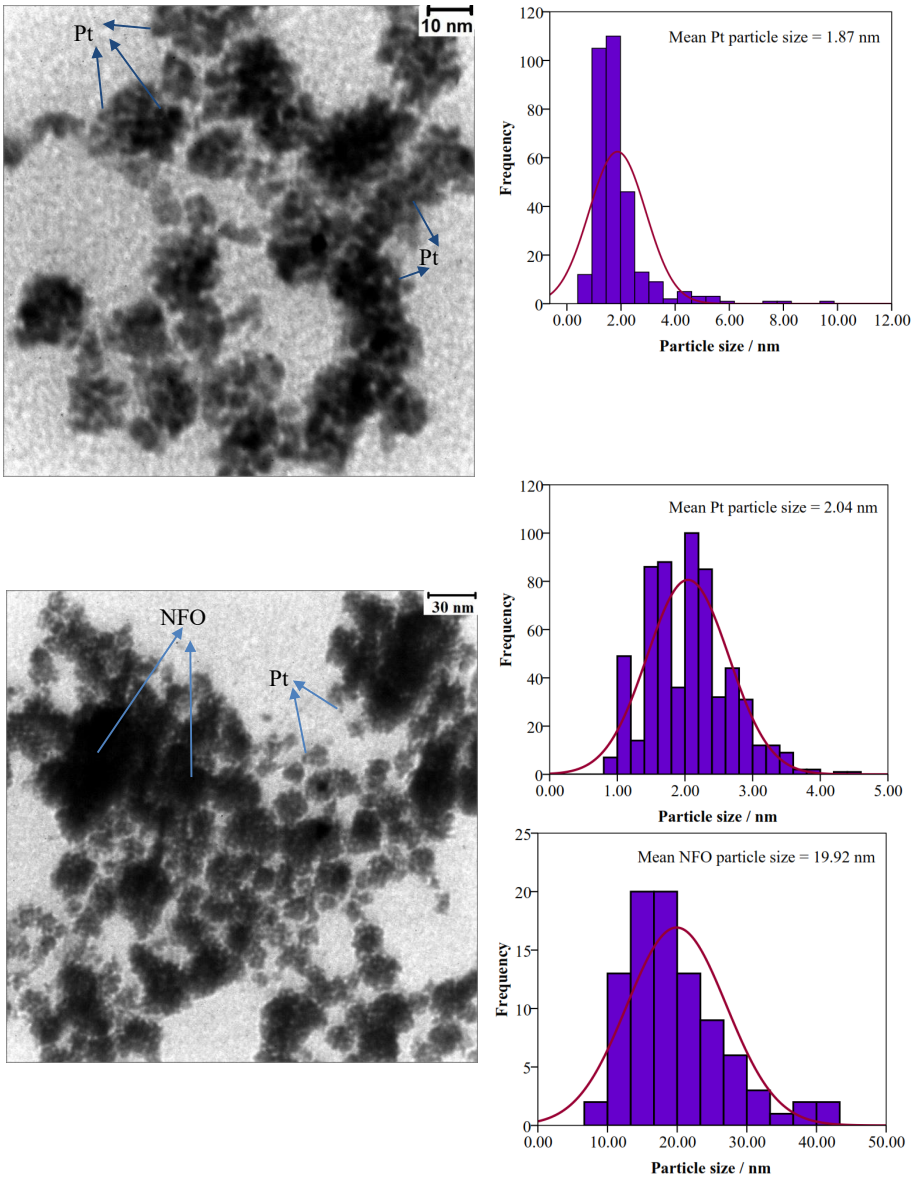

Fig. 3. TEM images of Pt/PA-CH and Pt-NFO/PA-CH catalysts.

was observed at 0.527 V whereas, for Pt/PA-CH catalyst, it was observed at 0.701 V. The onset potential for oxidation of the adsorbed CO at Pt/PA-CH and Pt-NFO/PA-CH catalysts were 0.574 V and 0.212 V, respectively. The onset and peak potential for oxidation of the adsorbed CO at Pt-NFO/PA-CH were much lower than Pt/PA-CH indicated that the adsorbed CO at the Pt-NFO/PA-CH surface is oxidized and removed more easily than that of Pt/PA-CH. Pt-NFO/PA-CH had higher CO tolerance than Pt/PA-CH [74, 75].

The catalytic performance of Pt-NFO/PA-CH, Pt/PA-CH and Pt/PA catalysts for methanol electro-oxidation was studied through the CV curves in 0.5 M H_2SO_4 and 1.68 M methanol solution at 100 mV s^{-1}. As depicted in Fig. 7A, NFO/PA-CH and PA-CH (not shown) GC modified electrodes showed no current peak for methanol electro-oxidation, therefore these electrodes had no electrocatalytic performance for MOR.

The CV curves of the synthesized catalysts exhibited two remarkable peaks for MOR. The peaks in the forward scans (I_f) were corresponded to methanol electro-oxidation and the peaks in

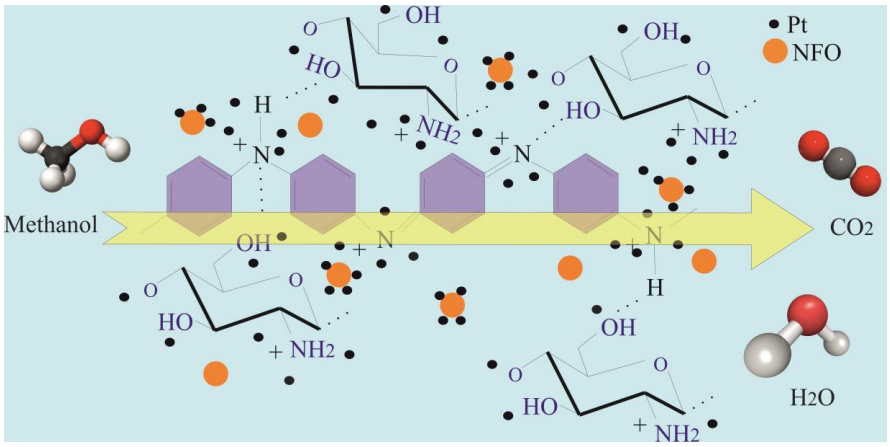

Fig. 4. The schematic illustration for preparing Pt-NFO/PA-CH nanocatalyst towards MOR.

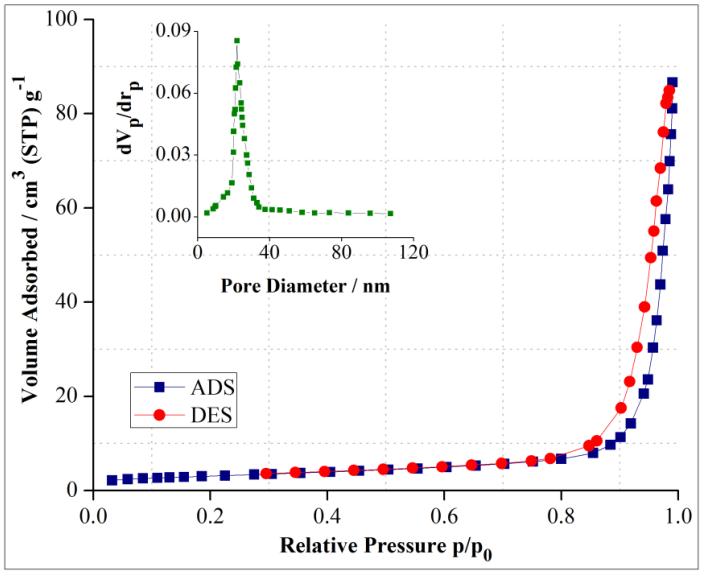

Fig. 5 N_2 adsorption–desorption isotherm and pore size distribution of NFO nanoparticles.

the backward scans (I_b) represented the oxidation of the adsorbed CO-containing species produced during MOR [76]. All the currents in Fig. 7A were mass normalized. For Pt-NFO/PA-CH and Pt/PA-CH catalysts, the anodic MOR peaks were located in the forward scan at 0.932 V and 0.766 V, respectively with the corresponding mass current of 15.755 and 5.151 A mg^{-1}_{Pt}. The second MOR peaks for Pt-NFO/PA-CH and Pt/PA-CH were observed in the backward scan around 0.622 V and 0.461 V, respectively. The electrochemical data of MO on the synthesized catalysts was summarized in Table 1. Magnitude of the anodic mass current indicated the catalytic activity for methanol electro-oxidation. As observed in Fig. 7A and Table 1, there was a great increase in the anodic mass current of Pt-NFO/PA-CH compared to Pt/PA-CH catalyst, suggesting that Pt-NFO/PA-CH has superior electrocatalytic ability for methanol electro-oxidation compared to Pt/PA-CH. The use of NFO nanoparticles accompanied by Pt nanoparticles significantly improved their catalytic activity for MOR. Catalytic activity of Pt/PA catalyst without using chitosan was also investigated for

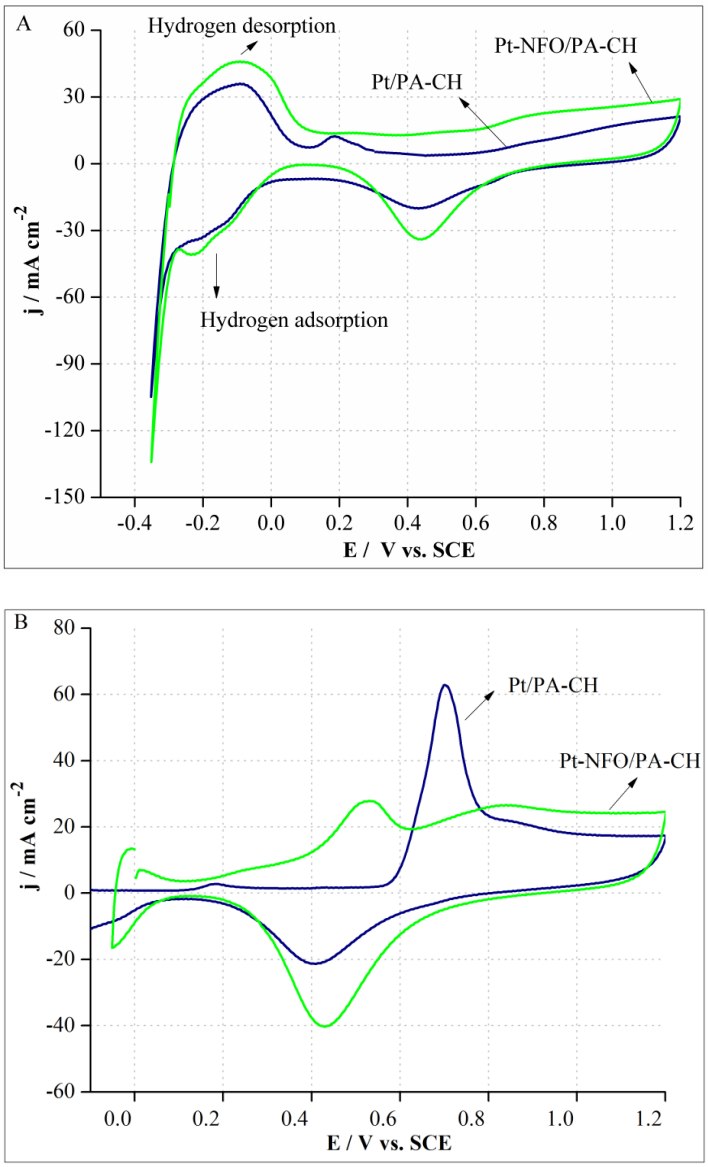

Fig. 6. A) CV curves, and B) CO absorption oxidation curves of Pt/PA-CH and Pt-NFO/PA-CH catalysts in H_2SO_4 0.5 M solution.

MOR compared to Pt/PA-CH catalyst. As shown in Fig. 7A, Pt/PA-CH had a little better catalytic activity than Pt/PA. The main advantage of using chitosan is improved dispersion of Pt nanoparticles and better adherence of the catalyst ink on the electrode's surface. The catalytic activity of Pt-NFO/PA-CH catalyst was compared with different catalysts prepared in the previous works (Table 2) [4, 76-78]. As shown in Table 2, Pt-NFO/PA-CH has higher catalytic activity than other catalysts towards MO according to its higher EAS and higher anodic mass current.

The long-term stabilities of Pt-NFO/PA-CH and Pt/PA-CH catalysts for MOR were measured by chronoamperometry (CA) technique. The CA curves were obtained in 0.5 M H_2SO_4 and 1.68 M methanol at 0.8 V vs. SCE for 1000 s (Fig. 7B). As shown in Fig. 7B, Pt-NFO/PA-CH had better catalytic activity than Pt/PA-CH for methanol electro-oxidation. Initially, the current of the prepared catalysts decreased rapidly. This may be related to the reactive intermediates generated during methanol electro-oxidation [79]. At the initial stage, Pt-NFO/PA-CH had a higher anodic

mass current (6.933 A mg^{-1}_{Pt}) compared to Pt/PA-CH (3.690 A mg^{-1}_{Pt}). After the measured time (1000 s), Pt-NFO/PA-CH (0.710 A mg^{-1}_{Pt}) still had higher current (approximately 2.8 times) than Pt/PA-CH (0.254 A mg^{-1}_{Pt}) indicating the higher tolerance of Pt-NFO/PA-CH to the produced intermediates (for example CO) during methanol electro-oxidation [80]. This result confirmed the enhanced catalytic performance of Pt/NFO/PA-CH compared to Pt/PA-CH for MOR.

Furthermore, electrochemical impedance spectroscopy (EIS) of the prepared electrodes was obtained to determine their behaviors for MOR [81]. EIS investigations were performed in 1.68 M methanol and 0.5 M H_2SO_4 at open circuit potential (OCP) and the frequency range of 1×10^4 to 10^{-2} Hz. The Nyquist plots of Pt/PA-CH and Pt-NFO/PA-CH catalysts are shown in Fig. 8. As can be seen, each Nyquist plot consists two parts of Z' and Z'' which represent the ohmic and capacitive parameters, respectively [82]. As illustrated in Fig. 8, Pt-NFO/PA-CH catalysts showed a smaller value of the semicircle diameter in the high frequency region compared to Pt/PA-CH indicating that Pt-NFO/PA-CH had lower charge transfer resistance at the electrode/electrolyte interface and better

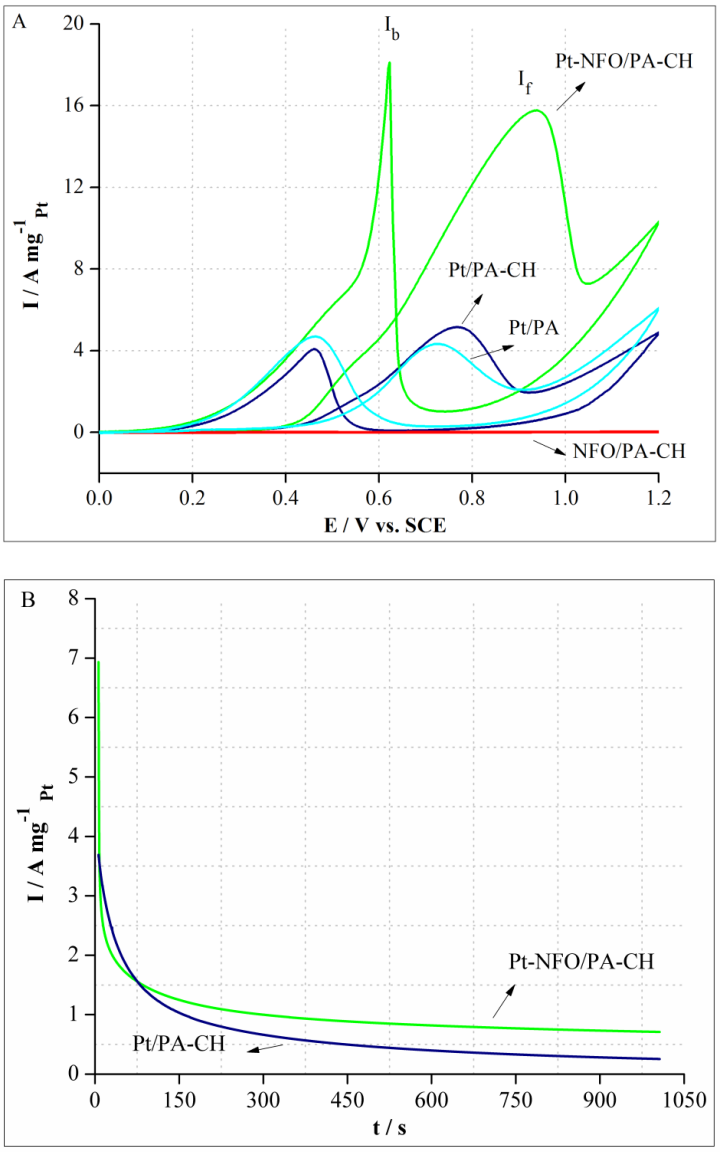

Fig. 7. A) CV curves and B) Chronoamperometry curves of catalysts in 0.5 M H_2SO_4 and 1.68 M methanol.

Table 1. Electrochemical data of methanol electro-oxidation at the prepared catalysts in 0.5 M H_2SO_4 and 1.68 M methanol solution

catalyst	E_{f1} (V)	I_{f1} (A mg^{-1}_{Pt})	E_b (V)	I_b (A mg^{-1}_{Pt})
Pt/PA	0.728	4.331	0.466	4.693
Pt/PA-CH	0.766	5.151	0.461	4.081
Pt-NFO/PA-CH	0.932	15.755	0.622	18.121

Table 2 Electrochemical data of methanol electro-oxidation at various catalysts.

Catalysts	EAS ($m^2 g^{-1}_{Pt}$)	E_f (V) vs. SCE	j_f (A mg^{-1}_{Pt})	E_b (V) vs. SCE	j_b (A mg^{-1}_{Pt})	ref
Pt/MV-RGO	24.65	0.63	0.221	0.47	0.225	[77]
Pt/RGO	8.25	0.63	0.084	0.50	0.071	[77]
RGO-PDMAEMA-Pt/Ag nanoscrolls	89.1	0.71	0.046	0.57	0.047	[76]
RGOPDMAEMA-Pt/Ag sheets	69.8	0.71	0.036	0.57	0.042	[76]
Pt/C	75	0.63	0.145	0.5	0.149	[78]
Pt/CrN	82	0.65	0.195	0.53	0.200	[78]
Pt/PVA/CH	5.40	0.668	0.191	0.405	0.118	[4]
Pt/PVA-CuO-Co_3O_4/CH	54.56	0.810	3.010	0.512	2.471	[4]
Pt/PVA-CuO-Co_3O_4	35.89	0.744	1.597	0.495	1.319	[4]
Pt/PA-CH	75.83	0.766	5.151	0.461	4.081	This work
Pt-NFO/PA-CH	94.46	0.932	15.755	0.622	18.121	This work

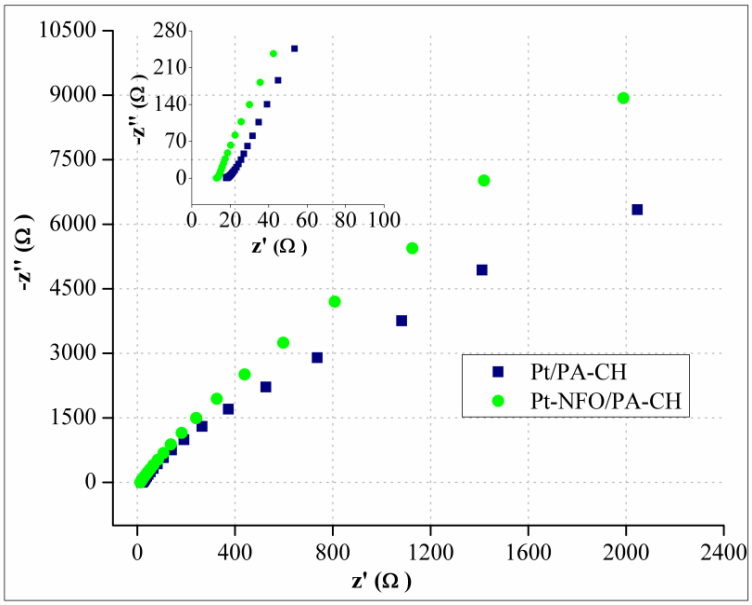

Fig. 8. Nyquist plots of Pt/PA-CH and Pt-NFO/PA-CH catalysts in 0.5 M H_2SO_4 and 1.68 M methanol.

conductivity than Pt/PA-CH [83]. A more vertical straight line at the EIS plot of Pt-NFO/PA-CH than that of Pt/PA-CH in the low frequency region revealed the improved ions diffusion feature of Pt-NFO/PA-CH for methanol electro-oxidation [69].

Temperature is an effective factor to get information about the reaction rate. To investigate the catalytic performance of Pt/PA-CH and Pt-NFO/PA-CH in different temperatures, cyclic voltammetry experiments were performed in 1.68 M methanol and 0.5 M H_2SO_4 in the temperature range of 28-45 ˚C (Fig. 9). As demonstrated, the anodic current densities of the prepared catalysts increase with temperature. Perhaps, this effect is

due to the increase in charge (ion) transfer rate at the interface of electrolyte and electrodes [84]. When the temperature increased from 28 to 45 ˚C, j_f increased from 123.625 to 296.672 mA cm^{-2} at Pt/PA-CH catalyst whereas, for Pt-NFO/PA-CH catalyst, j_f increased from 594.801 to 922.428 mA cm^{-2}. The activation energies (E_a) of the anodic peaks of methanol oxidation at Pt/PA-CH and Pt-NFO/PA-CH catalysts were determined according to the Arrhenius relationship (equation 2) and the suitable linear fit log j versus T^{-1} (Fig. 10) [84]:

$$I = Ae^{-E_a/RT} \quad (2)$$

In this equation, E_a defines activation energy, R is known as gas constant, I and T denote the current at the specific potential and temperature, respectively. The activation energies for Pt/PA-CH and Pt-NFO/PA-CH catalysts were 17.394 and 9.080 kJ mol^{-1}, respectively. The smaller value of activation energy of the anodic peak of MOR at Pt-NFO/PA-CH compared to Pt/PA-CH catalyst, revealing the faster charge transfer on the Pt-NFO/PA-CH surface [33, 71].

The catalytic activities of Pt/PA-CH and Pt-NFO/PA-CH catalysts for methanol electro-oxidation are shown at different scan rates (30-190 mVs^{-1}) in 0.5 M H_2SO_4 and 1.68 M methanol (Fig. 11). Increasing the scan rate resulted in increasing the anodic peak current of MOR with a positive shift in peak potential. As demonstrated in Fig. 11,

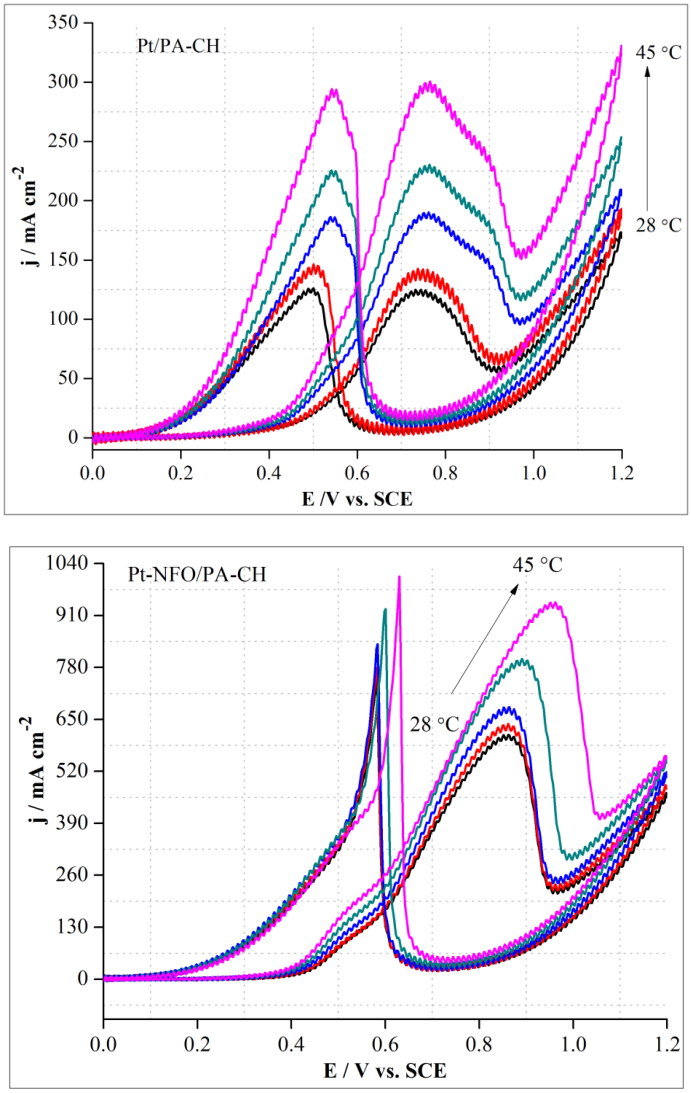

Fig. 9. CV curves of A) Pt-NFO/PA-CH and B) Pt/PA-CH catalysts at various temperatures of 28, 30, 35, 40, and 45 ˚C in 0.5 M H_2SO_4 and 1.68 M methanol.

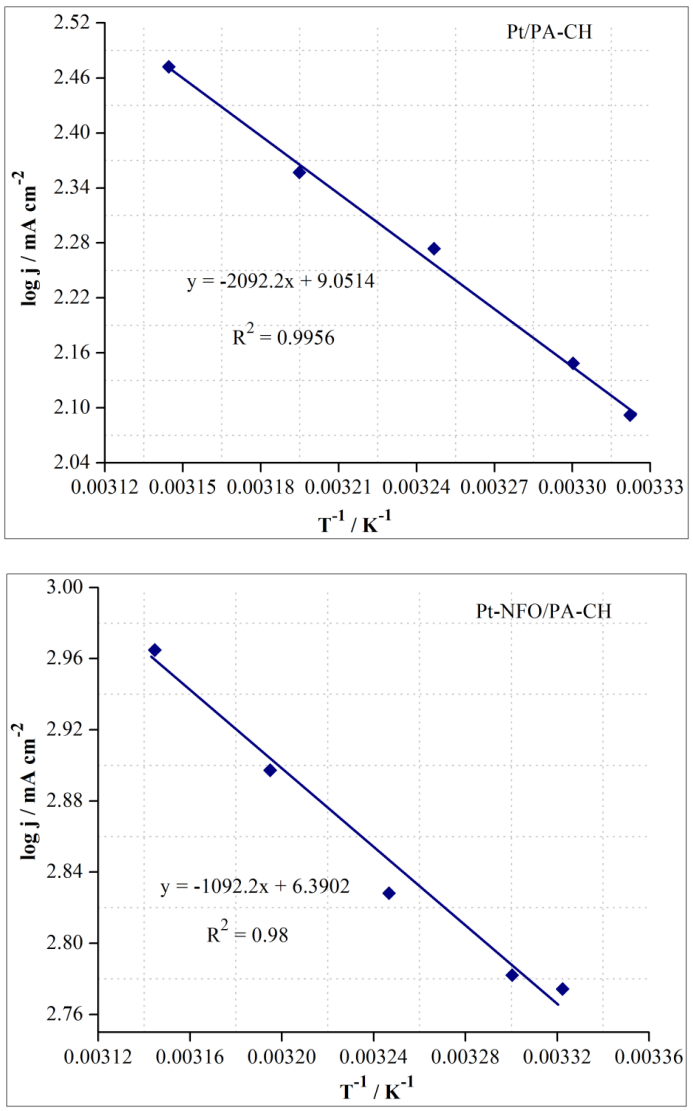

Fig. 10. Arrhenius plots for Pt-NFO/PA-CH and Pt/PA-CH catalysts towards methanol oxidation.

the anodic peak current densities of the catalysts (j_f) increase linearly with the square root of scan rate ($\upsilon^{0.5}$), which suggests that diffusion process is predominant during MOR [85]. Furthermore, the linear relationship between E_f and ln υ at Pt/PA-CH (R^2 = 0.94) and Pt-NFO/PA-CH (R^2 = 0.98) demonstrate that the kinetics is controlled by the surface reactions and indicates that MOR is an irreversible-diffusion process [86-88].

Fig. 12 represents the performance of Pt-NFO/PA-CH towards electro-oxidation of methanol with different concentrations in 0.5 M H_2SO_4 solution. As demonstrated in Fig. 12, anodic current of MOR increases with increase in methanol concentration and levels off at methanol concentrations more than 1.68 M. This effect is assumed to be occurred by saturation of active sites at the electrode's surface [70, 89]. Furthermore, when the concentration of methanol increases from 0.08 to 1.9 M, E_f shifts towards more positive potentials from 0.659 to 0.947 V. Perhaps, this effect is observed because of the following reason: the poisoning rate of Pt nanoparticles increases with increase in methanol concentration, thus the adsorbed intermediates at the Pt nanoparticles' surface would be removed at more positive potentials [90].

The long-term stabilities of Pt-NFO/PA-CH and Pt/PA-CH were studied through multiple CVs

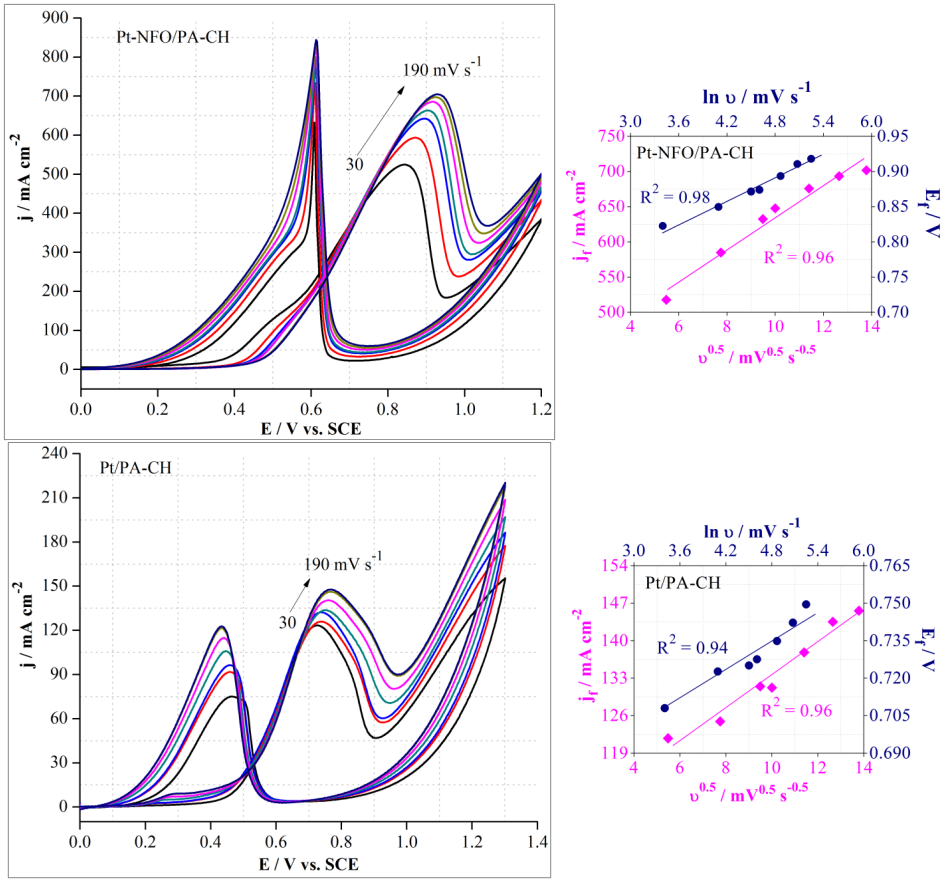

Fig. 11. CV curves of MOR at Pt/PA-CH and Pt-NFO/PA-CH catalysts at different scan rates (30, 60, 90, 100, 130, 160, and 190 mV s-1) in 1.68 M methanol and 0.5 M H_2SO_4. The anodic peak current density (jf) vs. square root of scan rate (υ0.5), and the anodic peak potential (Ef) vs. lnυ are also shown for the prepared catalysts.

tests (100 cycles) shown in Fig. 13. At Pt-NFO/PA-CH catalyst, j_f decreased to 79.66% of its initial value after 100 cycles. At Pt/PA-CH catalyst, j_f decreased to 79.41% of the original value after 100 cycles. As can be seen, Pt-NFO/PA-CH catalyst had a little better cycling stability for methanol electro-oxidation compared to Pt/PA-CH. Both of the prepared catalysts had good durability for methanol oxidation. Pt-NFO/PA-CH catalyst revealed much better catalytic performance for methanol electro-oxidation compared to Pt/PA-CH regarding the anodic current density [72, 91].

To study the kinetics of Pt/PA-CH and Pt-NFO/PA-CH catalysts, Tafel plots were considered using potentiodynamic pseudo-steady state polarization of 1.68 M CH_3OH in 0.5M H_2SO_4 solution at the scan rate of 30 mV s^{-1} shown in Fig. 14. Splitting of the first C-H bond of methanol with the first electron transfer is the rate-determining step of MOR [92]. The Tafel slopes of Pt/PA-CH and Pt-NFO/PA-CH were 249 and 234 mV.dec^{-1} respectively, indicating that methanol dehydrogenation reaction on Pt-NFO/PA-CH is faster than Pt/PA-CH.

The kinetic parameters of methanol oxidation for the prepared catalysts were calculated from the following Tafel equations (3) and (4) [93]:

$$\eta = a + b \log i \quad (3)$$

$$\eta = -\frac{2.303\ RT}{n\alpha F}\log i_0 + \frac{2.303\ RT}{n\alpha F}\log i \quad (4)$$

Where R is the gas constant, T is the temperature, i_0 is the exchange current density, F is the Faraday constant, α is the charge transfer coefficient.

The charge transfer coefficients of Pt/PA-CH and Pt-NFO/PA-CH were 0.23 and 0.25, respectively. The exchange current density for Pt/PA-CH and Pt-NFO/PA-CH catalysts was 0.19 and 0.31, respectively. The higher charge transfer

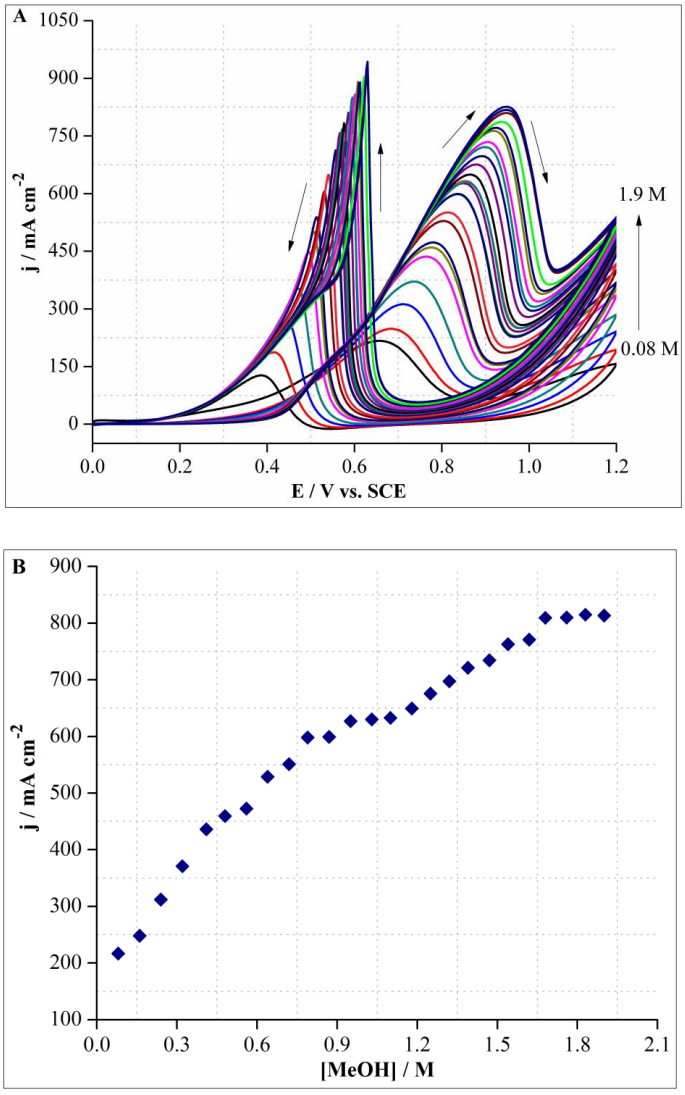

Fig. 12. CV curves of MOR at Pt-NFO/PA-CH catalyst in 0.5 M H_2SO_4 and various concentrations of methanol: 0.08, 0.16, 0.24, 0.32, 0.41, 0.48, 0.56, 0.64, 0.72, 0.79, 0.87, 0.95, 1.03, 1.1, 1.18, 1.25, 1.32, 1.39, 1.47, 1.54, 1.62, 1.68, 1.76, 1.83, 1.9 M.

coefficient, higher exchange current density and lower Tafel slope of Pt-NFO/PA-CH catalyst confirm its greater catalytic activity than Pt/PA-CH.

CONCLUSIONS

In this study, a novel Pt-NFO/PA-CH nanocatalyst was successfully synthesized and characterized. The catalytic activity of this catalyst was evaluated for methanol electro-oxidation and compared with that of Pt/PA-CH nanocatalyst. High catalytic performance of the prepared catalysts for methanol oxidation is probably attributed to the use of polyaniline and chitosan as support for nanoparticles. The use of PA and CH with their positive functional groups as catalyst support caused the uniform distribution of Pt nanoparticles confirmed with TEM images. Pt-NFO/PA-CH catalyst exhibited enhanced catalytic performance for methanol electro-oxidation compared to Pt/PA-CH, considering its better antipoisoning effect, improved electrochemically active surface area, higher long-term stability, better durability and higher anodic mass current for methanol oxidation than Pt/PA-CH. The use of NFO nanoparticles accompanied by Pt nanoparticles significantly enhanced their catalytic activity for MOR. Also,

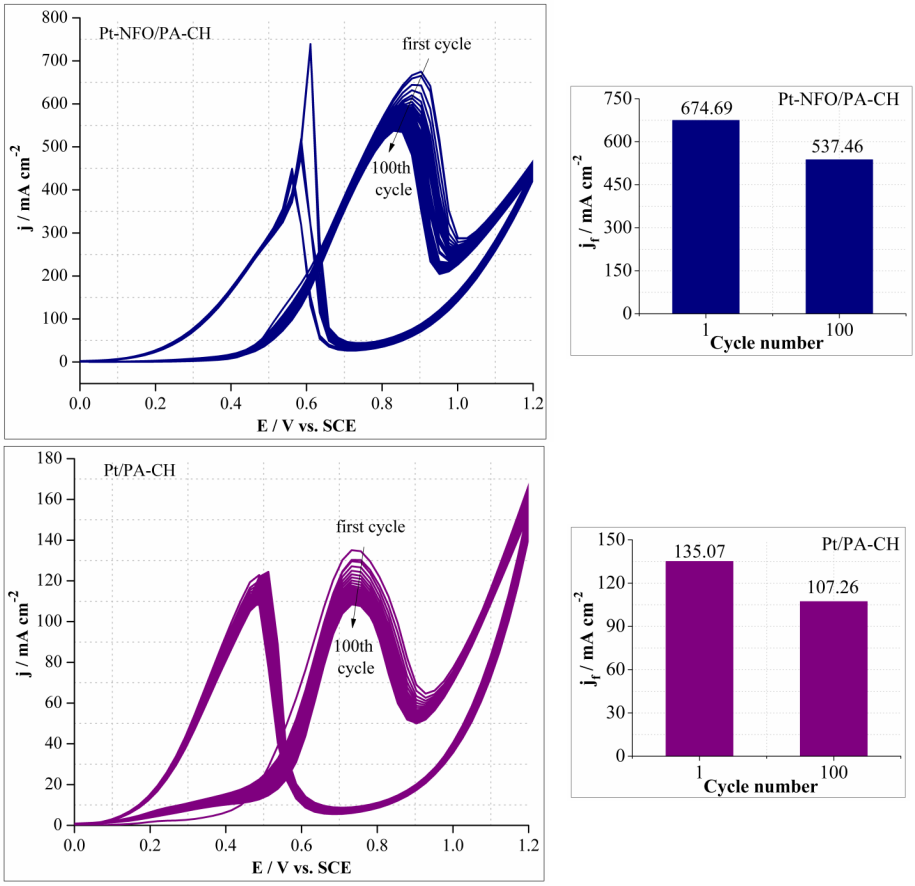

Fig. 13. CV curves of Pt/PA-CH and Pt-NFO/PA-CH catalysts during 100 cycles in 1.68 M methanol and 0.5 M H_2SO_4 solution. Anodic current densities of MO at the prepared catalysts are also shown as a function of cycle number.

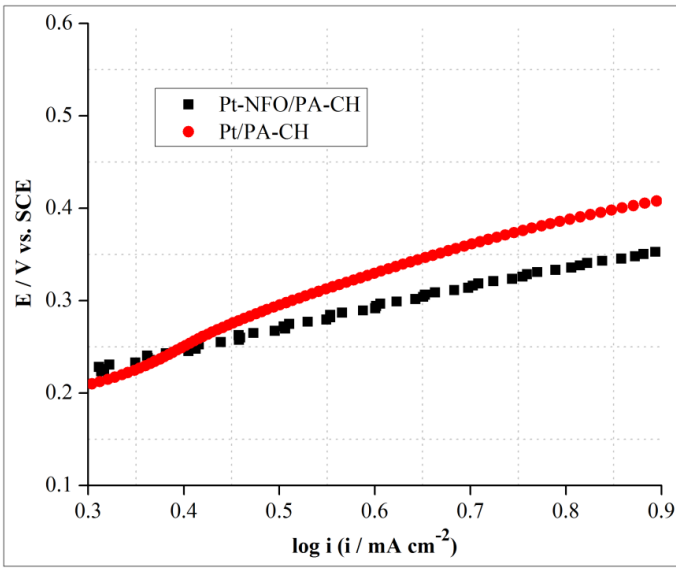

Fig. 14. Tafel plots for methanol oxidation on the prepared catalysts in 0.5 M H_2SO_4 and 1.68 M CH_3OH at 25˚C.

the presence of CH led to the excellent adherence of the catalyst ink over the GC working electrode. These investigations revealed that Pt-NFO/PA-CH can be utilized as an effective catalyst for methanol oxidation.

ACKNOWLEDGMENT

Technical and financial support of this work is provided by Payame Noor University of Mashhad, Esfarayen University of Technology, and Islamic Azad University of Zahedan for the presentation of S. Khammarnia's doctoral thesis.

CONFLICT OF INTEREST

The authors declare that there is no conflict of interests regarding the publication of this manuscript.

REFERENCES

1. Akyıldırım O, Yüksek H, Saral H, Ermiş İ, Eren T, Lütfi Yola M. Platinum nanoparticles supported on nitrogen and sulfur-doped reduced graphene oxide nanomaterial as highly active electrocatalysts for methanol oxidation. J Mater Sci Mater Electon, 2016; 27: 8559-8566.
2. Wang Y, Yang J, Sun S, Wang L, Guo T, Zhang D, Xue Z, Zhou X. PtNi nanoparticles supported on electrochemically reduced porous graphene oxide for methanol oxidation reaction. Chem Phys Lett, 2019; 730: 575-581.
3. Muneendra Prasad A, Santhosh C, Nirmala Grace A. Carbon nanotubes and polyaniline supported Pt nanoparticles for methanol oxidation towards DMFC applications. Appl Nanosci, 2012; 2: 457-466.
4. Ekrami-Kakhki MS, Naeimi A, Donyagard F. Pt nanoparticles supported on a novel electrospun polyvinyl alcohol-CuO-Co_3O_4/chitosan based on Sesbania sesban plant as an electrocatalyst for direct methanol fuel cells. Int J Hydrogen Energy, 2019; 44: 1671-1685.
5. An M, Du C, Du L, Sun Y, Wang Y, Chen C, Han G, Yin G, Gao Y. Phosphorus-doped graphene support to enhance electrocatalysis of methanol oxidation reaction on platinum nanoparticles. Chem Phys Lett, 2017; 687: 1-8.
6. Kumar S, Mahajan M, Singh R, Mahajan A. Silver nanoparticles anchored reduced graphene oxide for enhanced electrocatalytic activity towards methanol oxidation. Chem Phys Lett, 2018; 693: 23-27.
7. Saral H, Akyıldırım O, Yüksek H, Eren T. Platinum nanoparticles involved on nitrogen and sulfur-doped nanomaterial as fuel cell electrode. J Mater Sci Mater Electon, 2017; 28: 2691-2696.
8. Yuan J, Wang Z, Zhang Y, Shen YF, Han D, Zhang Q, Xu X, Niu L. Electrostatic layer-by-layer a of platinum-loaded multiwall carbon nanotube multilayer: A tunable catalyst film for anodic methanol oxidation. Thin Solid Films 2008; 516: 6531-6535.
9. Zheng Y, Zhang Z, Zhang X, Ni H, Sun Y, Lou Y, Li X, Lu Y. Application of Pt-Co nanoparticles supported on CeO_2-C as electrocatalyst for direct methanol fuel cell. Mater Lett, 2018; 221: 301-304.
10. Hunt ST, Milina M, Alba-Rubio AC, Hendon CH, Dumesic JA, Romn-Leshkov Y. Self-assembly of noble metal monolayers on transition metal carbide nanoparticle catalysts. Science, 2016; 352: 974-978.
11. Kakati N, Maiti J, Lee SH, Jee SH, Viswanathan B, Yoon YS. Anode catalysts for direct methanol fuel cells in acidic media: do we have any alternative for Pt or Pt-Ru. Chem Rev, 2014; 114: 12397-12429.
12. Li Y, Han L, An B, Wang Y, Wang L, Yin X, Lu J. Preparation of platinum catalysts supported on functionalized graphene and the electrocatalytic properties for ethanol oxidation in direct ethanol fuel cell. J Mater Sci Mater Electon, 2016; 27: 6208-6215.
13. Teran FE, Santos DM, Ribeiro J, Kokoh KB. Activity of PtSnRh/C nanoparticles for the electrooxidation of C1 and C2 alcohols. Thin Solid Films 2012; 520: 5846-5850.
14. Wang YJ, Zhao N, Fang B, Li H, Bi XT, Wang H. Carbon supported Pt-based alloy electrocatalysts for the oxygen reduction reaction in polymer electrolyte membrane fuel cells: particle size, shape, and composition manipulation and their impact to activity. Chem Rev, 2015; 115: 3433-3467.
15. Chou HY, Hsieh CK, Tsai MC, Wei YH, Yeh TK, Tsai CH. Pulse electrodeposition of Pt and Pt–Ru methanol-oxidation nanocatalysts onto carbon nanotubes in citric acid aqueous solutions. Thin Solid Films 2015; 584: 98-102.
16. Jiang K, Shao Q, Zhao D, Bu L, Guo J, Huang X. Phase and composition tuning of 1D platinum-nickel nanostructures for highly efficient electrocatalysis. Adv Funct Mater, 2017; 27: 1700830.
17. Ekrami-Kakhki MS, Farzaneh N, Abbasi S, Beitollahi H, Ekrami-Kakhki SA. An investigation of methyl viologen functionalized reduced graphene oxide: chitosan as a support for Pt nanoparticles towards ethanol electrooxidation. Electron Mater Lett, 2018; 14: 616-628.
18. Jayaraman S, Jaramillo TF, Baeck SH, McFarland EW. Synthesis and characterization of Pt-WO_3 as methanol oxidation catalysts for fuel cells. J Phys Chem B, 2005; 109: 22958-22966.
19. Yao KS, Chen YC, Chao CH, Wang WF, Lien SY, Shih HC, Chen TL, Weng KW. Electrical enhancement of DMFC by Pt–M/C catalyst-assisted PVD. Thin Solid Films 2010; 518: 7225-7228.
20. Suntivich J, Xu Z, Carlton CE, Kim J, Han B, Lee SW, Bonnet N, Marzari N, Allard LF, Gasteiger HA, Hamad-Schifferli K, Shao-Horn Y. Surface composition tuning of Au-Pt bimetallic nanoparticles for enhanced carbon monoxide and methanol electro-oxidation. J Am Chem Soc, 2013; 135: 7985-7991.
21. Chang Q, Xu Y, Duan Z, Xiao F, Fu F, Hong Y, Kim J, Choi SI, Su D, Shao M. Structural evolution of sub-10 nm octahedral platinum-nickel bimetallic nanocrystals. Nano Lett, 2017; 17: 3926-3931.
22. Wang P, Zhang X, Zhang J, Wan S, Guo S, Lu G, Yao J, Huang X. Precise tuning in platinum-nickel/nickel sulfide interface nanowires for synergistic hydrogen evolution catalysis. Nat Commun, 2017; 8: 1-9.
23. Cao Z, Chen Q, Zhang J, Li H, Jiang Y, Shen S, Fu G, Lu BA, Xie Z, Zheng L. Platinum-nickel alloy excavated nano-multipods with hexagonal close-packed structure and superior activity towards hydrogen evolution reaction. Nat Commun, 2017; 8: 1-7.
24. Jia Y, Jiang Y, Zhang J, Zhang L, Chen Q, Xie Z, Zheng L. Unique excavated rhombic dodecahedral $PtCu_3$ alloy nanocrystals

constructed with ultrathin nanosheets of high-energy {110} facets. J Am Chem Soc, 2014; 136: 3748-3751.
25. Chen Q, Yang Y, Cao Z, Kuang Q, Du G, Jiang Y, Xie Z, Zheng L. Excavated cubic platinum-tin alloy nanocrystals constructed from ultrathin nanosheets with enhanced electrocatalytic activity. Angew Chem Int Edit, 2016; 55: 9021-9025.
26. Li J, Rong H, Tong X, Wang P, Chen T, Wang Z. Platinum-silver alloyed octahedral nanocrystals as electrocatalyst for methanol oxidation reaction. J Colloid Interf Sci, 2017; 513: 251-257.
27. Mylswamy S, Wang CY, Liu RS, Lee J-F, Tang M-J, Lee J-J, Weng B-J. Anode catalysts for enhanced methanol oxidation: An in situ XANES study of PtRu/C and PtMo/C catalysts. Chem Phys Lett, 2005; 412: 444-448.
28. Ekrami-Kakhki MS, Yavari Z, Saffari J, Abbasi S. Fabrication and evaluation of Pt/M (M= Co, Fe) chitosan supported catalysts for methanol electrooxidation: application in direct alcohol fuel cell. J Nanostruct, 2016; 6: 221-234.
29. Patel PP, Datta MK, Jampani PH, Hong D, Poston JA, Manivannan A, Kumta PN. High performance and durable nanostructured Tin supported Pt_{50}-Ru_{50} anode catalyst for direct methanol fuel cell (DMFC). J Power Sources, 2015; 293: 437-446.
30. Zaidi SJ, Bello M, Al-Ahmed A, Yousaf AB, Imran M. Mesoporous carbon supported Pt/MO_2 (M = Ce, Pr, Nd, Sm) heteronanostructure: Promising non-Ru methanol oxidation reaction catalysts for direct methanol fuel cell application. J Electroanal Chem, 2017; 794: 86-92.
31. Amin RS, Abdel Hameed RM, El-Khatib KM, El-Abd H, Souaya ER. Effect of preparation conditions on the performance of nano Pt–CuO/C electrocatalysts for methanol electro-oxidation. Int J Hydrogen Energy, 2012; 37: 18870-18881.
32. Tang Z, Lu G. High performance rare earth oxides LnO_x (Ln=Sc, Y, La, Ce, Pr and Nd) modified Pt/C electrocatalysts for methanol electrooxidation. J Power Sources, 2006; 162: 1067-1072.
33. Eshghi A, kheirmand M, Sabzehmeidani MM. Platinum-iron nanoparticles supported on reduced graphene oxide as an improved catalyst for methanol electro oxidation. Int J Hydrogen Energy, 2018; 43: 6107-6116.
34. Chen Y, Wang D, Qin H, Zhang H, Zhang Z, Zhou G, Gao C, Hu J. CO_2 sensing properties and mechanism of $PrFeO_3$ and $NdFeO_3$ thick film sensor. J Rare Earths, 2019; 37: 80-87.
35. Wu Z, Zhang R, Zhao M, Fang S, Han Z, Hu J, Wang K. Effect of Pd doping on the acetone-sensing properties of $NdFeO_3$. Int J Min Met Mater, 2012; 19: 141-145.
36. Yavari Z, Noroozifar M, Khorasani-Motlagh M. Presentation of anodic electrocatalyst for polymeric fuel cell: Pt nanoparticles immobilized on $NdFeO_3$ nanocrystals and carbon nanotubes. Indian J Chem Technol, 2019; 26: 9-22.
37. Yavari Z, Noroozifar M, Parvizi T. Performance evaluation of anodic nano-catalyst for direct methanol alkaline fuel cell. Environ Prog Sustain, 2018; 37: 597-604.
38. Ghosh D, Kim SO. Chemically modified graphene based supercapacitors for flexible and miniature devices. Electron Mater Lett, 2015; 11: 719-734.
39. Lee SH, Jeong GH. Effect of catalytic metals on diameter-controlled growth of single-walled carbon nanotubes: Comparison between Fe and Au. Electron Mater Lett, 2012; 8: 5-9.
40. Gao H, He L, Zhang Y, Zhang S, Wang L. Facile synthesis of Pt nanoparticles supported on graphene/vulcan XC-72 carbon and their application for methanol oxidation. Ionics, 2017; 23: 435-442.
41. Ekrami-Kakhki MS, Farzaneh N, Fathi E. Superior electrocatalytic activity of Pt-$SrCoO_{3-\delta}$ nanoparticles supported on functionalized reduced graphene oxide-chitosan for ethanol oxidation. Int J Hydrogen Energy, 2017; 42: 21131-21145.
42. Takahashi M, Mori T, Vinu A, Ou DR, Kobayashi H, Drennan J. Development of high quality Pt–CeO_2 electrodes supported on carbon black for direct methanol fuel cell applications. Adv Appl Ceram, 2008; 107: 57-63.
43. Tang H, Chen J, Nie L, Liu D, Deng W, Kuang Y, Yao S. High dispersion and electrocatalytic properties of platinum nanoparticles on graphitic carbon nanofibers (GCNFs). J Colloid Interf Sci, 2004; 269: 26-31.
44. Zhang Y, Li F, Liu X, Chen H, Luo Y, Jing L, Lu J, Zhang G. Methanol electrocatalytic oxidation on Pt/Poly(o-toluidine) film/activated carbon doped graphite carbon paste electrode. Chem J Chin Univ, 2017; 38: 2320-2327.
45. Hu ZA, Ren LJ, Feng XJ, Wang YP, Yang YY, Shi J, Mo LP, Lei ZQ. Platinum-modified polyaniline/polysulfone composite film electrodes and their electro catalytic activity for methanol oxidation. Electrochem Commun, 2007; 9: 97-102.
46. Eris S, Dasdelen Z, Yildiz Y, Sen F. Nanostructured polyaniline-rGO decorated platinum catalyst with enhanced activity and durability for Methanol oxidation. Int J Hydrogen Energy, 2018; 43: 1337-1343.
47. Zhang G, Tan L, Cheng H, Li F, Liu X, Lu J. Different interesting enhanced influence from polyaniline and poly(o-toluidine) on electrocatalytic activities of Pt on them toward electrooxidation of methanol. Int J Hydrogen Energy, 2018; 43: 16049-16060.
48. Khuspe GD, Navale ST, Bandgar DK, Sakhare RD, Chougule MA, Patil VB. SnO_2 nanoparticles-modified polyaniline films as highly selective, sensitive, reproducible and stable ammonia sensors. Electron Mater Lett, 2014; 10: 191-197.
49. Yan R, Jin B, Li D, Zheng J, Li Y, Qian C. One-step electrochemically co-deposited Pt nanoparticles/polyaniline composites with raspberry structures for methanol electro-oxidation. Synth Met, 2018; 235: 110-114.
50. Profeti D, Olivi P. Methanol electrooxidation on platinum microparticles electrodeposited on poly (o-methoxyaniline) films. Electrochim Acta, 2004; 49: 4979-4985.
51. Yin F, Wang D, Zhang Z, Zhang C, Zhang Y. Synthesis of mesoporous hollow polypyrrole spheres and the utilization as supports of high loading of Pt nanoparticles. Mater Lett, 2017; 207: 225-229.
52. Merati Z, Basiri Parsa J, Babaei-Sati R. Electrochemically synthesized polypyrrole/MWCNTs-Al_2O_3 ternary nanocomposites supported Pt nanoparticles toward methanol oxidation. Int J Hydrogen energy, 2018; 43: 20993-21005.
53. Carrillo I, Leo TJ, Santiago O, Acción F, Moreno-Gordaliza E, Raso MA. Polypyrrole and platinum deposited onto carbon substrate to enhance direct methanol fuel cell electrodes behavior. Int J Hydrogen Energy, 2018; 43: 16913-16921.
54. Prodromidis MI, Zahran EM, Tzakos AG, Bachas LG. Preorganized composite material of polyaniline–palladium nanoparticles with high electrocatalytic activity to methanol and ethanol oxidation. Int J Hydrogen Energy, 2015; 40: 6745-6753.

55. Zhang Q, Lv JN, Hu XY, He YL, Yang HF, Kong DS, Feng YY. Polyaniline decorated MoO_3 nanorods: Synthesis, characterization and promoting effect to Pt electrocatalyst. Int J hydrogen Energy, 2018; 43: 5603-5609.
56. Mondal S, Malik S. Easy synthesis approach of Pt-nanoparticles on polyaniline surface: an efficient electro-catalyst for methanol oxidation reaction. J Power Sources, 2016; 328: 271-279.
57. Guibal E. Heterogeneous catalysis on chitosan-based materials: a review. Prog Polym Sci, 2005; 30: 71-109.
58. Ye JR, Zhai S, Gu ZJ, Wang N, Wang H, Shen Q. Electro-synthesis and characterization of polyaniline nanofibers. Mater Lett, 2014; 132: 377-379.
59. Dong JQ, Shen Q. Enhancement in solubility and conductivity of polyaniline with lignosulfonate modified carbon nanotube. J Polym Sci B Polym Phys, 2009; 47: 2036-2046.
60. Dong JQ, Shen Q. Comparison of polyanilines doped by lignosulfonates with three different ions. J Appl Polym Sci, 2012; 126: E10-E16.
61. Gu ZJ, Wang JT, Li LL, Chen LF, Shen Q. Formation of polyaniline nanotubes with different pore shapes using α-, β- and γ-cyclodextrins as templates. Mater Lett, 2014; 117: 66-68.
62. Gu ZJ, Ye JR, Song W, Shen Q. Synthesis of polyaniline nanotubes with controlled rectangular or square pore shape. Mater Lett, 2014; 121: 12-14.
63. Kung CC, Lin PY, Xue Y, Akolkar R, Dai L, Yu X, Liu CC. Three dimensional graphene foam supported platinum–ruthenium bimetallic nanocatalysts for direct methanol and direct ethanol fuel cell applications. J Power Sources, 2014; 256: 329-335.
64. Khorasani-Motlagh M, Noroozifar M, Ahanin-Jan A. Ultrasonic and microwave assisted co-precipitation synthesis of pure phase $LaFeO_3$ perovskite nanocrystals. J Iran Chem Soc, 2012; 9: 833-839.
65. Shanker J, Rao GN, Venkataramana K, Babu DS. Investigation of structural and electrical properties of $NdFeO_3$ perovskite nanocrystalline. Phys Lett A, 2018; 382: 2974-2977.
66. Brunauer S, Emmett PH, Teller E. Adsorption of gases in multimolecular layers. J Am Chem Soc, 1938; 60: 309-319.
67. Barrett EP, Joyner LG, Halenda PP. The determination of pore volume and area distributions in porous substances. I. computations from nitrogen isotherms. J Am Chem Soc, 1951; 73: 373-380.
68. Noroozifar M, Khorasani-Motlagh M, Ekrami-Kakhki MS, Khaleghian-Moghadam R. Enhanced electrocatalytic properties of Pt-chitosan nanocomposite for direct methanol fuel cell by $LaFeO_3$ and carbon nanotube. J Power Sources, 2014; 248: 130-139.
69. Kakaei K, Rahimi A, Husseindoost S, Hamidi M, Javan H, Balavandi A. Fabrication of Pt-CeO_2 nanoparticles supported sulfonated reduced graphene oxide as an efficient electrocatalyst for ethanol oxidation. Int J Hydrogen Energy, 2016; 41: 3861-3869.
70. Ekrami-Kakhki MS, Farzaneh N, Abbasi S, Makiabadi B. Electrocatalytic activity of Pt nanoparticles supported on novel functionalized reduced graphene oxide-chitosan for methanol electrooxidation. J Mater Sci: Mater Electron, 2017; 28: 12373-12382.
71. Shafaei Douk A, Saravani H, Noroozifar M. One-pot synthesis of ultrasmall Pt-Ag nanoparticles decorated on graphene as a high-performance catalyst toward methanol oxidation. Int J Hydrogen Energy, 2018; 43: 7946-7955.
72. Wang H, Xue Y, Zhu B, Yang J, Wang L, Tan X, Wang Z, Chu Y. CeO_2 nanowires stretch-embedded in reduced graphite oxide nanocomposite support for Pt nanoparticles as potential electrocatalyst for methanol oxidation reaction. Int J Hydrogen Energy, 2017; 42: 20549-20559.
73. Alcaide F, Alvarez G, Cabot PL, Grande HJ, Miguel O, Querejeta A. Testing of carbon supported Pd–Pt electrocatalysts for methanol electrooxidation in direct methanol fuel cells. Int J Hydrogen Energy, 2011; 36: 4432-4439.
74. Feng G, Pan Z, Xu Y, Chen H, Xia G, Zhang Y, Shi S, Deng X. Platinum decorated mesoporous titanium cobalt nitride nanorods catalyst with promising activity and CO-tolerance for methanol oxidation reaction. Int J Hydrogen Energy, 2018; 43: 17064-17068.
75. Moniri S, Van Cleve T, Linic S. Pitfalls and best practices in measurements of the electrochemical surface area of platinum-based nanostructured electro-catalysts. J Catal, 2017; 345: 1-10.
76. Jin X, Wang X, Zhang Y, Wang H, Yang Y. Reduced graphene oxide-poly-(2-(dimethylamino) ethyl methacrylate)-Pt/Ag nanoscrolls and its electrocatalytic performance for oxidation of methanol. Int J Hydrogen Energy, 2018; 43: 13440-13449.
77. Ma J, Wang L, Mu X, Cao Y. Enhanced electrocatalytic activity of Pt nanoparticles supported on functionalized graphene for methanol oxidation and oxygen reduction. J Colloid Interf Sci, 2015; 457: 102-107.
78. Yang M, Guarecuco R, DiSalvo FJ. Mesoporous chromium nitride as high performance catalyst support for methanol electrooxidation. Chem Mater, 2013; 25: 1783-1787.
79. Zhang F, Wang Z, Xu KQ, Xia J, Liu Q, Wang Z. Highly dispersed ultrafine Pt nanoparticles on nickel-cobalt layered double hydroxide nanoarray for enhanced electrocatalytic methanol oxidation. Int J Hydrogen Energy, 2018; 43: 16302-16310.
80. Li XT, Lei H, Yang C, Zhang QB. Electrochemical fabrication of ultra-low loading Pt decorated porous nickel frameworks as efficient catalysts for methanol electrooxidation in alkaline medium. J Power Sources, 2018; 396: 64-72.
81. Silva CD, Morais LH, Gonçalves R, Matos R, Souza GLC, Freitas RG, Pereira EC. The methanol and CO electro-oxidation onto Pt_{pc}/Co/Pt metallic multilayer nanostructured electrodes: An experimental and theoretical approach. Electrochim Acta, 2018; 280: 197-205.
82. Nadeem M, Yasin G, Bhatti MH, Mehmoodd M, Arif M, Dai L. Pt-M bimetallic nanoparticles (M = Ni, Cu, Er) supported on metal organic framework-derived N-doped nanostructured carbon for hydrogen evolution and oxygen evolution reaction. J Power Sources, 2018; 402: 34-42.
83. Volkan Özdokur K, Bozkurt Çırak B, Caglar B, Çırak Ç, Morkoç Karadeniz S, Kılınç T, Erdoğan Y, Ercan Ekinci A. Fabrication of TiO_2/ZnO/Pt nanocomposite electrode with enhanced electrocatalytic activity for methanol oxidation. Vacuum, 2018; 155: 242-248.
84. Shafaei Douk A, Saravani H, Noroozifar M. A fast method to prepare Pd-Co nanostructures decorated on graphene as excellent electrocatalyst toward formic acid oxidation. J Alloy Comp, 2018; 739: 882-891.
85. Zhao Y, Yang X, Tian J, Wang F, Zhan L. Highly dispersed Pd nanoparticles on 2-aminophenoxazin-3-one functionalized MWCNTs surface for methanol electro-oxidation in alkaline

media. Mater Sci Eng B Solid State Mater Adv Technol, 2010; 171: 109-115.
86. Estudillo-Wong LA, Santillan-Dıaz G, Arce-Estrada EM, Alonso-Vante N, Manzo-Robledo A. Electroreduction of NOx species in alkaline medium on Pt nanoparticles. Electrochim Acta, 2013; 88: 358-364.
87. Danaee I, Jafarian M, Forouzandeh F, Gobal F, Mahjani MG. Electrocatalytic oxidation of methanol on Ni and NiCu alloy modified glassy carbon electrode. Int J Hydrogen Energy, 2008; 33: 4367-4376.
88. Ali S, Khan I, Khan SA, Sohail M, Ahmed R, Rehman A, Shahid Ansari M, Morsy MA. Electrocatalytic performance of Ni@Pt core-shell nanoparticles supported on carbon nanotubes for methanol oxidation reaction. J Electroanal Chem, 2017; 795: 17-25.
89. Zhang K, Chen X, Wang L, Zhang D, Xue Z, Zhou X, Lu X. Pt-Pd nanoparticles supported on sulfonated nitrogen sulfur co-doped graphene for methanol electro-oxidation. Int J Hydrogen Energy, 2018; 43: 15931-15940.
90. Abdel Rahim MA, Abdel Hameed RM, Khalil MW. Nickel as a catalyst for electro-oxidation of methanol in alkaline medium. J Power Sources, 2004; 134: 160-169.
91. Chang G, Cai Z, Jia H, Zhang Z, Liu Z, Zhu R, He Y, Liu X. High electrocatalytic performance of a graphene-supported PtAu nanoalloy for methanol oxidation. Int J Hydrogen Energy, 2018; 43: 12803-12810.
92. Fang YH, Liu ZP. First principles Tafel kinetics of methanol oxidation on Pt(111). Surf Sci, 2015; 631: 42-47.
93. Ghosh S, Bera S, Bysakh S, Basu RN. Conducting polymer nanofiber-supported Pt alloys: unprecedented materials for methanol oxidation with enhanced electrocatalytic performance and stability. Sustain. Energy Fuels, 2017; 1: 1148-1161.